Available online at www.sciencedirect.com
SCIENCE DIRECT®
Journal of Catalysis 234 (2005) 421–430
JOURNAL OF CATALYSIS
www.elsevier.com/locate/jcat

Study of the influence of the In_2O_3 loading on γ-alumina for the development of de-NO_x catalysts

J.A. Perdigon-Melon [a,b], A. Gervasini [c], A. Auroux [a,*]

[a] *Institut de Recherches sur la Catalyse, CNRS, 2 avenue Einstein, 69626 Villeurbanne cedex, France*
[b] *Instituto de Química-Física "Rocasolano", CSIC, c/ Serrano 119, 28006 Madrid, Spain*
[c] *Dipartimento di Chimica Fisica ed Elettrochimica, Università degli Studi di Milano, via C. Golgi n.19, 20133 Milano, Italy*

Received 16 May 2005; revised 25 June 2005; accepted 3 July 2005

Available online 11 August 2005

Abstract

Alumina-supported indium oxide (In_2O_3) catalysts with In loadings between 2 and 22 wt% were prepared by impregnation and characterized for their main properties. Surface properties, such as the surface area; surface In content, measured by X-ray photoelectron spectroscopy (XPS); and acidity and basicity, measured both by adsorption microcalorimetry using ammonia and sulfur dioxide as probe molecules and by infrared spectroscopy of pyridine adsorption, were determined. Bulk properties, namely the crystallographic structure as determined by powder X-ray diffraction (XRD) analysis and the redox character of the In_2O_3-dispersed phase as determined by redox cycles performed both in a flow apparatus and in a thermobalance coupled with a differential scanning microcalorimeter (TG-DSC), were studied. The results obtained were interpreted in terms of In_2O_3 surface dispersion or aggregation. The catalysts tested in the reduction of NO_x by ethene in an oxygen-rich atmosphere showed an interesting ability to selectively reduce NO_x to N_2, independently of the In loading. The weakness of the oxidative properties of the In_2O_3 phases limited the ethene combustion and made the catalysts able to reduce NO_x even at high temperature (up to 550 °C). The rates of nitrogen formation depended strongly on the In_2O_3 aggregation state; the In centers were very active even at low amounts.

Keywords: Alumina-supported indium oxide; de-NO_x catalysts; Surface characterizations; Redox and acid/base sites

1. Introduction

Catalysts containing group III elements (B, Al, Ga, and In) have received much attention in recent years [1–13]. Besides their use as supports for active metal centers, particularly in Al_2O_3-containing materials, these elements play an important role in novel catalytic materials such as promoters, supported metal oxides and mixed oxides, supported bimetallic catalysts, and modified zeolites [14–24]. These catalysts have been tested in various catalytic reactions of petrochemical (e.g., aromatization of light alkanes and dehydrogenation of long-chain alkanes) and environmental interest. In this direction, the search for viable catalysts that can selectively reduce nitrogen oxides (NO_x) in an oxidizing environment has been underway for many years [8,9,14,15]. Since the first reports of the high selective catalytic reduction and decomposition activity toward NO_x of copper- [25,26] and other cations (Fe, Co, Ga, and In) [24,27–30]-exchanged zeolites, a large variety of nonzeolitic, practically usable, catalysts have been tested for the NO abatement of emissions from both motor vehicles and stationary sources under net oxidizing conditions.

Gallium or indium supported on zeolites have been found to be more suitable for the de-NO_x reactions (i.e., selective catalytic reduction of NO_x by using hydrocarbons, HC-SCR process) than copper or iron, which favor the undesired direct complete oxidation of the used hydrocarbon species to carbon dioxide rather than the hydrocarbon oxidation by the NO_x species [24,27,31]. Moreover, it has recently been

* Corresponding author. Fax: +33-472445399.
E-mail address: auroux@catalyse.cnrs.fr (A. Auroux).

0021-9517/$ – see front matter
doi:10.1016/j.jcat.2005.07.001

demonstrated that Ga_2O_3 and In_2O_3 oxides supported on acidic supports, such as γ-Al_2O_3, TiO_2, and SiO_2–Al_2O_3, present a remarkable de-NO_x catalytic activity [13,32–36]. Low-loading In_2O_3 catalysts supported on alumina have been reported to show not only high-activity NO_x reduction, but also high resistance to water and SO_2 poisoning [12,37], which makes them innovative and promising catalytic materials for de-NO_x applications.

Although promising catalytic results have been obtained and in-depth characterization studies on In_2O_3 on alumina-based catalysts have been performed in the last few years [5,32,37,38], the detailed properties of such materials in relation to the presence of surface acidic and/or basic species and indium redox character merit further attention due to their high implication in the reactivity. In this paper, a series of In_2O_3-oxide based catalysts with different loadings (3–30 wt%) supported on a commercial γ-Al_2O_3 were prepared and studied in terms of their surface and bulk properties and catalytic activity. The acidic character of these catalysts and the effect of acidity on their activity and selectivity have been studied. The combined use of Fourier transform infrared (FTIR) spectroscopy and adsorption microcalorimetry made it possible to characterize the acid–base properties of the samples. FTIR spectroscopy of adsorbed pyridine gave information on the types of acidic sites present, whereas adsorption microcalorimetry of NH_3 and SO_2 probe molecules gave the number and strength of the acidic and basic sites, respectively. The understanding of the surface chemistry of such systems also requires deeper insight into the redox character of the active sites. The information derived from the characterization techniques has been correlated with the NO_x reduction activity in catalytic tests carried out under lean conditions and high space velocity. We conclude that the In aggregation state at the surface and the relative redox properties play a decisive role in the de-NO_x reaction.

2. Experimental

2.1. Sample preparation

Samples with different amounts of indium oxide supported on γ-Al_2O_3 (oxide C from Degussa) have been prepared by incipient wetness impregnation using appropriate amounts of $In(NO_3)_3{\cdot}5H_2O$ from Aldrich (99.9%). After impregnation, the samples were dried at 120 °C overnight and calcined at 500 °C in oxygen flow for 12 h. The amount of indium oxide varied from 3 to 24 wt%. Bulk In_2O_3 was prepared in the same way, by calcination of indium nitrate at 500 °C after drying at 120 °C overnight.

2.2. Sample characterization

The concentrations of the supported indium oxide were determined by AES-ICP in a Spectroflame-ICP instrument. Surface areas were determined by the BET method from the adsorption of nitrogen at −196 °C. The crystallographic structure was examined by XRD in a Bruker (Siemens) D5005 apparatus (Cu-K_α radiation, 0.154 nm). The oxidation state of indium was determined by XPS at room temperature using an SSI 301 spectrometer.

The acidity and basicity of the supported indium samples and of the bare support were determined by adsorption microcalorimetry, using NH_3 and SO_2 as probe molecules. The measurements were carried out isothermically at 80 °C in a heat flow calorimeter (Setaram C80) coupled with a standard volumetric apparatus [39–42]. The samples were pretreated at 400 °C in vacuum overnight before the measurements were made. Successive doses of gas were sent to the sample until a final pressure of 0.5 Torr was obtained. The sample was then evacuated for 30 min at the same temperature to remove the amount physically adsorbed, and a second adsorption was performed. The quantity adsorbed at 0.2 Torr in the first adsorption is called V_T (total adsorbed amount). The difference between the amounts adsorbed in the first and second adsorptions at 0.2 Torr is the irreversibly chemisorbed amount (V_{irr}).

FTIR measurements were carried out in self-supported pellets in a Bruker Vector 22 spectrometer. Before these measurements, the samples were pretreated in oxygen flow at 400 °C overnight and pumped out for 1 h at the same temperature. For each sample, one spectrum was recorded on the clean sample, and a second spectrum was recorded after pyridine adsorption at room temperature and evacuation at 150 °C for 30 min.

The redox properties of the supported indium samples have been studied by TPR–TPO. The sample was held in a U-shaped quartz reactor, allowing the reductant or oxidizing gas stream to pass through the sample. In TPR experiments, the temperature was increased by 5 °C min^{-1} from room temperature up to 840 °C, under a reducing atmosphere of 5% H_2/Ar (flux 20 $cm^3\,min^{-1}$). The temperature was kept at 840 °C for 1 h, then the sample was cooled under argon atmosphere. After TPR, a TPO experiment was carried out using the same experimental conditions but increasing the temperature only up to 800 °C, because volatilization of In_2O_3 occurs at 850 °C [43]. The oxidizing atmosphere was 1% O_2/He. The hydrogen or oxygen consumption was determined by means of a TCD (Delsi Instruments DN11). Before TPR experiments, the samples were reoxidized under oxygen at 400 °C for 3 h and cooled down under argon atmosphere.

The redox properties were also studied using a differential scanning calorimeter (DSC) coupled to a microbalance (TG-DSC 111 from Setaram). This equipment makes it possible not only to calculate the reduced or oxidized amount from the weight loss or gain of the sample, but also to simultaneously measure the evolved heat associated with the reduction or oxidation process. Unlike in the TPR–TPO experiments, the samples were held in a quartz crucible so the reactant gas could not pass through the sample. As in TPR–TPO, successive experiments of reduction and oxi-

dation were carried out. The temperature was increased at 5 °C min^{-1} up to 650 °C, then kept constant for 30 min before the samples were cooled under helium atmosphere. The reduction experiments were carried out using a total flux of 30 cm^3 min^{-1} with a mixture of 68% of hydrogen in helium. For oxidation experiments, the flux was 15 cm^3 min^{-1}, with a composition of 46% O_2/He.

2.3. Catalytic activity experiments

The catalytic tests were carried out with powder samples of mass around 0.1 g. The powders were introduced in a quartz tubular microreactor (5 mm i.d.) between plugs of quartz wool and pretreated in a flow containing 20% v/v of O_2/He while increasing the temperature in stages up to 350 °C and maintaining it for 4 h. The reactant stream was obtained using a set of mass flow controllers (Bronkhorst, Hi-Tec) supplying about 3000 ppm of NO and of C_2H_4, and 40,000 ppm of O_2 in helium at a total flow rate of 85 cm^3 min^{-1}, with the reactor at near-atmospheric pressure. The simultaneous presence in the feed mixture of NO with large amounts of O_2 gave rise to homogeneous oxidation of NO, leading to the presence of NO_2 in the feed (namely, NO_x) as well. The amount of NO_2 was typically about 16% of the NO total feed. Contact time was maintained constant at 1.6 g s mmol^{-1} (GHSV = 50,000 h^{-1}). The temperature was increased from 250 to 550 °C with a heating rate of 10 °C/min, and eight reaction temperatures were investigated in this interval. Each temperature plateau was maintained for 70 min. The attainment of steady-state conditions was controlled by recording the concentration of the different species as a function of time on stream (TOS). As a general trend, 30 min was a sufficient time to obtain stable concentrations of the different species.

The exit gas stream of the reactor flowed through a gas cell (multiple reflection gas cell, path length 2.4 m) in the beam of an FTIR spectrometer (Bio-Rad with a DTGS detector). The spectrometer made it possible to individuate and measure the concentrations of NO, N_2O, and NO_2 for N-containing species and of C_2H_4, CO, and CO_2 for C-containing species. The measurements were carried out with a resolution of 0.50 cm^{-1}, with an accumulation of 19 scans per spectrum. The gas cell presented an accuracy of ±10 ppm for NO and ±4 ppm for N_2O and for NO_2 using lines at 1876, 2225, and 1619 cm^{-1}, respectively. The cumulative absorbance of all the IR active species flowing from the reactor was monitored every 120 s. The absorbance profile of each species detected as a function of time or temperature of reaction was determined on the basis of the chosen wavelength of absorption of the species, decomposing the cumulative absorbance curve.

De-NO_x activity in terms of NO_x conversion was determined by subtracting the total NO + NO_2 concentration flowing out from the reactor from the total NO + NO_2 concentration fed into the reactor. The amount of NO_x converted corresponded to N_2 formed. From this determination, specific rates per unit mass of catalyst and per mol of In were calculated. Selectivity to N_2 was evaluated in terms of the so-called "competitiveness factor" (S_{SCR}, %), defined as the ratio between the amount of C_2H_4 consumed to reduce NO_x to N_2 and the total amount of C_2H_4 consumed [44,45].

3. Results and discussion

3.1. Characterization analysis

The indium oxide loading determined by chemical analysis and the surface area are summarized in Table 1. A remarkable decrease in the surface area occurred on increasing the amount of indium oxide deposited. The variation of the surface area of the different samples with the deposited indium oxide amount is represented in Fig. 1. The data fit very well with a straight line, indicating that the decrease in the surface area can be due to the coverage of the support by a phase of much lower surface area, rather than to a change of morphology or other modification of the support, due to blockage of its pores. Fig. 2 presents the XRD spectra of all the samples. Whereas the chosen alumina was an amorphous support, the bulk indium oxide presents very well-developed crystalline phases. The peak intensities and their 2θ angles were identified as characteristic of the cubic structure of In_2O_3. In the supported samples, the crystalline

Table 1
Physico-chemical properties of the samples

Sample	Surface area (m^2 g^{-1})	Loading (wt%)		XPS	
		In	In_2O_3	BE (eV)	In/Al molar ratio
Al_2O_3	112	0	0		
InAl-3	113	2.64	3.19		0.02
InAl-6	106	5.5	6.65	444.9	0.052
InAl-10	103	8.28	10.01	445	0.064
InAl-13	96	10.78	13.03	444.9	0.033
InAl-17	90	14.27	17.25	444.8	0.034
InAl-27	82	22.13	26.76	444.7	0.047
In_2O_3	21	82.71	100	444.5	

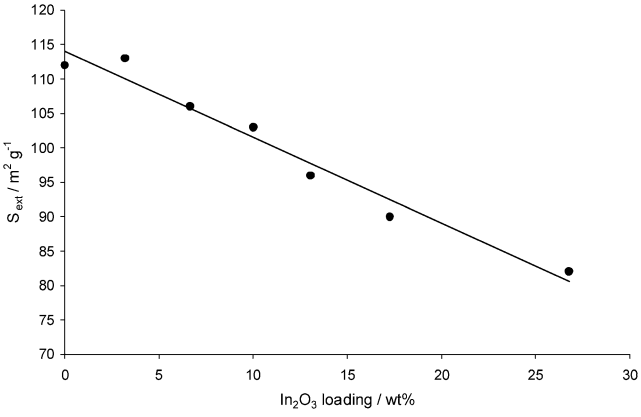

Fig. 1. Relation between sample surface area and indium oxide loading.

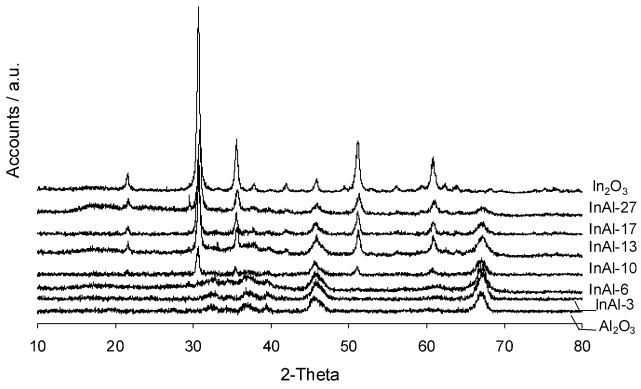

Fig. 2. XRD of the samples loaded with different amounts of indium oxide.

indium oxide phase was observed starting from 10% loading. The position of the line and the relative intensities of the signal were the same as for the bulk indium oxide, indicating that the support did not influence the crystallization of indium oxide. For the least-loaded samples (InAl-3 and InAl-6), no signal was observed due to the small crystal size or to the presence of amorphous indium oxide. In addition, sample InAl-17 displayed better dispersion than sample InAl-13.

XPS experiments make it possible to determine not only the oxidation state, but also the surface In/Al ratio. These results are summarized in Table 1. In all cases, only one oxidation state was found, with binding energy for In $3d_{5/2}$ between 444.5 and 444.8 eV. These values are characteristic of In_2O_3 [46]. Considering that XPS is a surface technique, the In/Al ratio gives an idea of the dispersion of the deposited oxide. The higher the ratio, the higher the amount of exposed indium oxide compared with the total amount of deposited indium oxide. Because the theoretical monolayer is around 23 wt% of InO_3 [8], increasing the In loading should have given rise to an increasing or at least constant In/Al ratio for a similar dispersion, but this was not the case. There was no direct relationship between the amount of deposited indium oxide and the In/Al ratio, because the maximum ratio was reached for the InAl-10 sample. Above 10 wt% of In_2O_3, the In/Al molar ratio decreased significantly without a clear trend with In loading. This may be because the high heterogeneity of the surfaces have more or less large zones of uncovered support. Moreover, it is likely that only a limited amount of alumina centers can act as anchoring points for bonding with indium oxide. Above 10 wt%, these centers appear to behave as nucleation or aggregation centers. Similar results have been found by other authors [37].

Fig. 3 shows the FTIR spectra of the supported indium samples and the bare alumina in the region of hydroxyl groups after pretreatment in oxygen flow at 400 °C and further outgassing at the same temperature. The typical OH vibrations at 3672, 3723, and 3788 cm^{-1} found for γ-Al_2O_3 [47] were not altered by the indium oxide deposition. A new signal not found in bare alumina appeared at 3766 cm^{-1} and

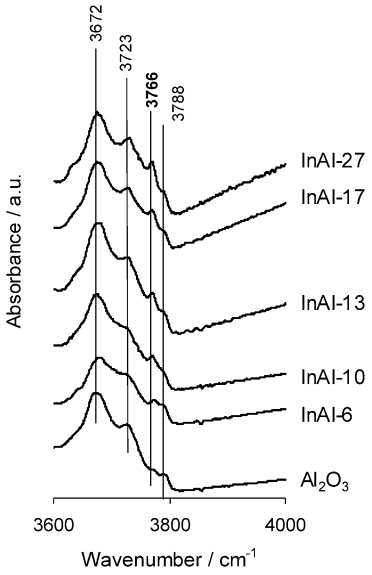

Fig. 3. FTIR spectra in the νOH region of the support and supported In_2O_3 samples after activation at 400 °C.

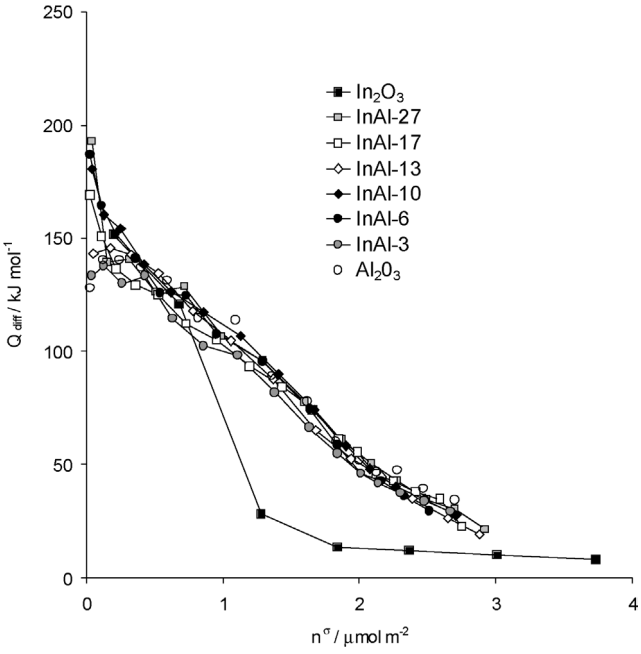

Fig. 4. Differential heats of ammonia adsorption vs coverage on indium oxide samples supported on alumina.

became more intense as the indium content increased. High-frequency OH groups are frequently attributed to basic sites.

The differential heats of ammonia adsorption versus coverage at 80 °C are represented in Fig. 4. To compare the ammonia-adsorbed amounts between the different samples, these amounts are represented per square meter of surface area. All the supported indium oxide samples present the same profile as bare alumina. Only a slight difference can be observed in the initial part of the curve, where the supported indium oxide samples present higher adsorption heats than the pure alumina, probably due to a charge imbalance along

Table 2
Total and irreversibly adsorbed amounts of ammonia and sulfur dioxide at 80 °C

Sample	NH_3 adsorbed amount ($\mu mol\ m^{-2}$)		SO_2 adsorbed amount ($\mu mol\ m^{-2}$)	
	V_T	V_{irr}	V_T	V_{irr}
Al_2O_3	2.40	1.44	1.94	1.69
InAl-3	2.35	1.47	1.90	1.64
InAl-6	2.20	1.38	2.30	2.05
InAl-10	2.41	1.48	2.37	2.11
InAl-13	2.44	1.42	2.07	1.80
InAl-17	2.33	1.51	2.28	1.97
InAl-27	2.51	1.52	2.43	2.11
In_2O_3	2.14	1.00	2.24	1.91

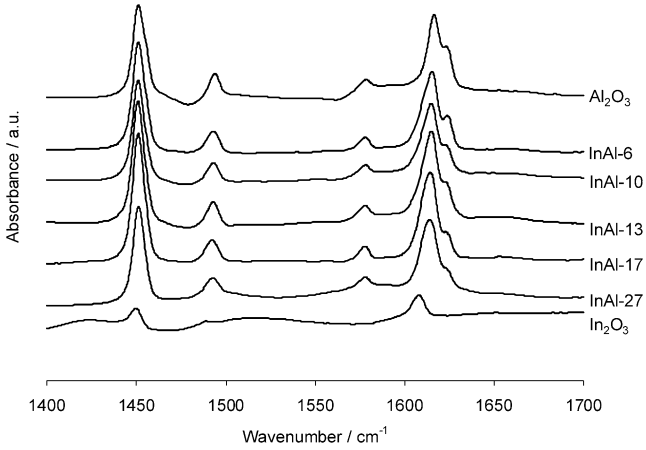

Fig. 5. FTIR spectra of pyridine after adsorption at room temperature and evacuation at 150 °C.

the Al–O–In linkages [48]. Bulk indium oxide is clearly the sample with the lowest amount of adsorbed ammonia. The total and irreversibly adsorbed amounts of ammonia are summarized in Table 2. Bulk indium oxide has the lowest irreversibly adsorbed amount, whereas the amounts for the other samples are very similar. Because the surface area decreases with increasing loading, a slight decrease in acidity would be observed if these numbers were calculated in $\mu mol\ g_{cat}^{-1}$ [8]. These results suggest that the amphoteric indium oxide can be considered more basic than acidic, and that the acidity of the supported samples is due mainly to alumina.

A similar trend is observed in the FTIR spectra of adsorbed pyridine (Fig. 5). Only bands characteristic of pyridine adsorbed on Lewis acid sites (1620–1600 cm^{-1} ν_{8a}, 1450 cm^{-1} ν_{19b}) are observed. The position and multiplicity of the ν_{8a} band of adsorbed pyridine is related to the strength and number of the different types of Lewis acid sites [6]. Although a slight shift toward lower wave numbers is observed after indium oxide deposition, no great differences in the position of this band can be observed among the catalysts, meaning that the strength of the Lewis acid sites is almost always the same. Bulk indium oxide presents the smallest band and the lowest wave number for pyridine adsorption,

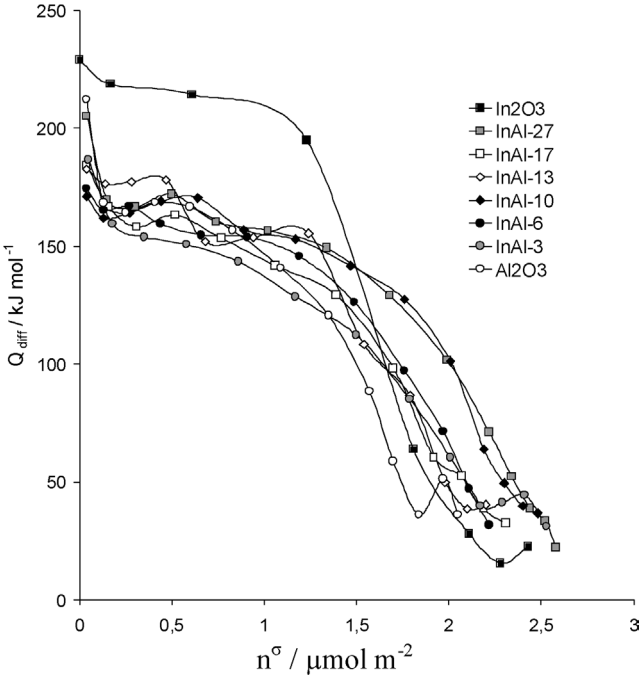

Fig. 6. Differential heats of sulfur dioxide adsorption versus coverage on indium oxide samples supported on alumina.

indicating the low acidity of this oxide. The doubled signal of the ν_{8a} band indicates the presence of two different types of acidic centers on the alumina support. The supported indium samples present the same behavior, but the relative area of the second band becomes lower as the indium oxide content increases, suggesting that these centers could be blocked by the indium oxide.

Fig. 6 represents the adsorption heats of SO_2 on all the samples. In contrast to ammonia adsorption, marked differences are observed among the different samples. Bulk indium oxide presents the highest adsorption heats of all the samples, again suggesting the main basic character of this oxide. A clearer idea can be obtained by observing the irreversibly adsorbed amounts of SO_2 (Table 2). No evident relation can be established between V_{irr} and the total indium oxide loading, but the samples with the highest In/Al ratios determined by XPS (Table 1)—namely InAl-10, InAl-6, and InAl-27—are those with the highest irreversibly adsorbed amounts, indicating a strong relation between surface indium oxide content and adsorbed amount.

The redox properties of the indium oxide materials supported on alumina were studied by TPR/TPO. The hydrogen consumptions and temperatures of the maximum of the reduction peaks are given in Table 3. The reduction profile of bulk indium oxide is represented in Fig. 7. A single and broad peak centered at 755 °C, incompletely finished, is obtained. The total reduction of In_2O_3 to In^0 requires 3 mol of hydrogen per mol of indium oxide. In the TPR experiment, the hydrogen consumption was 2.8 $mol_{H_2}\ mol_{In_2O_3}^{-1}$, indicating that almost all of the indium oxide has been reduced. The XRD spectra (not shown) recorded after TPR ex-

Table 3
Hydrogen/oxygen consumptions and peak maximum temperatures in TPR and TPO experiments

Sample	TPR			TPO		
	$mol_{H_2}\ mol^{-1}_{In_2O_3}$	T_{max} (°C)		$mol_{O_2}\ mol^{-1}_{In_2O_3}$	T_{max} (°C)	
Al_2O_3	–	–		–	–	
InAl-3	–	–		–	–	
InAl-6	2.2	295	560	n.d.	n.d.	
InAl-10	2.8	244	594	0.3	190	323
InAl-13	2.9	280	659	n.d.	n.d.	
InAl-17	2.8	275	699	0.8	200	345
InAl-27	2.6	230	713	0.9	200	337
In_2O_3	2.8		755	–	–	

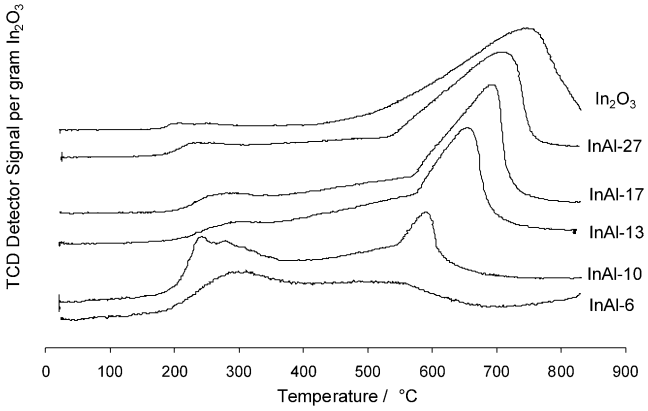

Fig. 7. TPR profiles of indium oxide samples supported on alumina.

periments show only the signal corresponding to a metallic indium phase. The supported indium samples with the highest indium oxide loadings (InAl-27, InAl-17, and InAl-13) present the same trend (Fig. 7), but in these cases low hydrogen consumption starting around 200 °C is observed until the main consumption begins, with this reduction amount at lower temperature becoming larger as the indium oxide content decreases. For sample InAl-10, the TPR profile presents the same trend, but the relative amount reduced at low temperature is more important, presenting a well-marked peak centered at 244 °C. For InAl-6, as in the case of InAl-10, the relative amount reduced at low temperature is more important than the amount reduced at high temperature. Because the reduction peak at low temperature does not appear in the TPR profile of bulk indium oxide, this peak can hardly be attributed to a different oxidation step in the reduction from In^{3+} to In^0. The reduction of bulk indium oxide to metallic indium seems to occur in one step [49], and the behavior observed for the supported oxides is generally attributed to the reduction of indium oxide particles of different sizes [37], with the smallest particles being reduced at low temperature. This conclusion fits well with the dispersion suggested by the XPS data. The reduced amount at low temperature is more important for the samples with the highest In/Al ratio (InAl-10 and InAl-6) than for the samples with poorer dispersion. In all cases, the reduced amount is nearly 100% of the indium content.

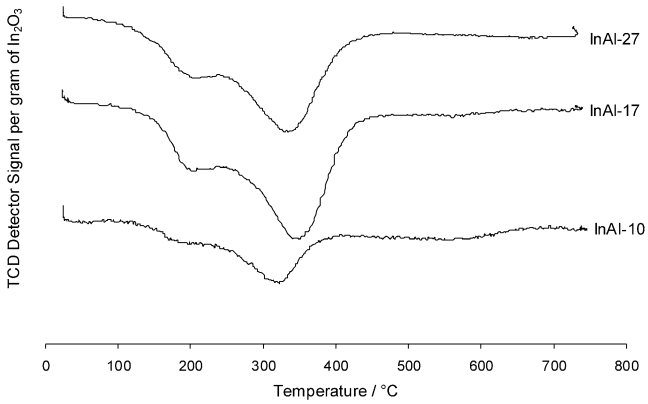

Fig. 8. TPO profiles of indium oxide samples supported on alumina.

TPO experiments were carried out on the reduced bulk indium oxide, InAl-27, InAl-17, and InAl-10. Bulk indium oxide did not show any oxygen consumption. Fig. 8 presents the TPO profiles for the three other samples. The three samples present the same profile, a double peak with an onset around 110 °C and the maximum around 320 °C (Table 3). The oxidation temperature is clearly lower than the reduction temperature. The amount of oxygen consumed per mol of indium oxide is given in Table 3. Assuming that the complete oxidation of In^0 to In_2O_3 requires 1.5 mol of oxygen per mol of indium, we can conclude that only part of the indium has been oxidized. Nevertheless, the only detected phase after TPO is indium oxide. One experiment of TPO on InAl-17 was stopped at 220 °C (before the main oxidation peaks) to see whether the first oxidation peak was due to intermediate oxidation states. The only phases found were In^0 and In_2O_3, suggesting that, as in the case of reduction, the presence of different peaks is related to the size of the reduced particle and not to oxidation in successive steps. The similitude of InAl-27 and InAl-17 is probably due to the phenomenon of sintering of the indium in the previous TPR experiment. The oxidation peak on InAl-10 occurs at a lower temperature.

To complement the TPR/TPO experiments, the redox properties of the supported indium oxide samples with the highest loadings, as well as bulk indium oxide, were studied by TG-DSC. Because of the different experimental conditions (composition of reactive gases, total flow or flow path), it is not possible to compare the two techniques quantitatively, but from a qualitative standpoint the results are similar. In reduction experiments (Fig. 9), only one endothermic peak is observed, at a reduction temperature that increases with increasing indium oxide loading. The experimental and theoretical mass losses are compared in Table 4. Values close to 100% are obtained, indicating that almost all of the indium oxide has been reduced. Values slightly exceeding 100% can be assigned to the presence of a small fraction of water or hydroxide. The measured reduction heats are also summarized in Table 4. Because these values are given per mol of indium oxide, a constant value could be expected a priori. As can be seen, the higher the indium oxide loading, the higher the measured heat, with the highest value for

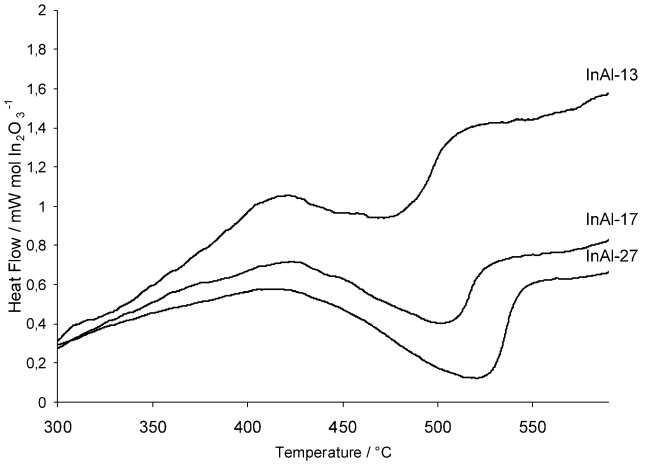

Fig. 9. DSC heat flow signal in reduction experiments.

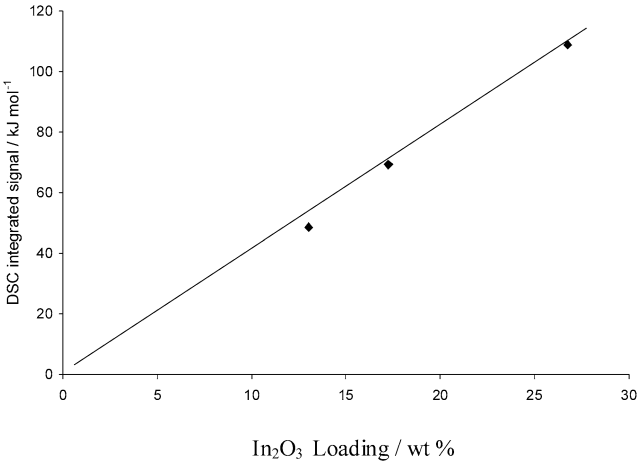

Fig. 10. Evolved heat in DSC reduction experiments versus indium oxide loading.

Table 4
Temperature of the maximum, evolved heat and mass variation in the reduction/oxidation experiments carried out by TG-DSC

Sample	Reduction			Oxidation		
	T_{max} (°C)	Heat[a] (kJ mol^{-1})	Δm[b] (%)	T_{max} (°C)	Heat[a] (kJ mol^{-1})	Δm[b] (%)
Al_2O_3	–	–	–	–	–	–
InAl-13	479	48.5	93	317	−149.7	113
InAl-17	501	69.3	95	318	−177.9	81
InAl-27	532	108.9	107	299	−203.8	107
In_2O_3	550	171.4	108	–	–	–

[a] Heat evolved per mol of indium oxide.
[b] Mass loss and gain relative to the theoretical one.

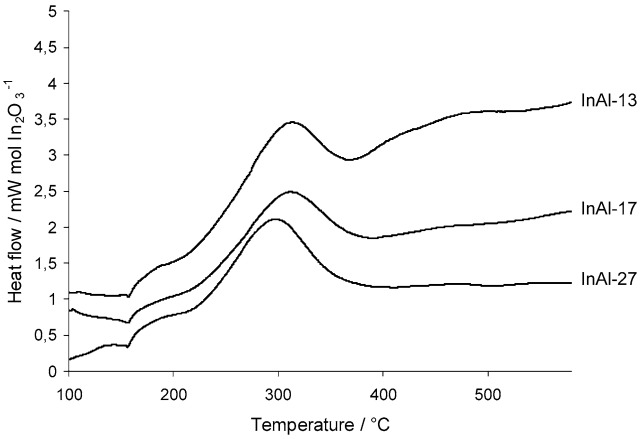

Fig. 11. Evolved heat in DSC in reoxidation experiments.

bulk indium oxide. In Fig. 10 the measured heat is represented versus the total amount of indium oxide deposited. A good linear relationship is obtained, suggesting that this variation of the measured heat with the loading is due to the influence of the support. At low loadings, strong interactions with the support lower the reduction heats. As in the TPR–TPO experiments, no reoxidation of bulk metallic indium is observed. Parallel to the TPR reoxidation experiments, a double exothermic peak is observed in the reoxidation experiments performed by DSC (Fig. 11). The maximum and onset of the reoxidation peaks for the three samples are more similar than they were in the reduction process, probably due to the sintering of indium in the reduction process, leading to a more similar dispersion of the three samples. The mass gain (Table 4) suggests that the metallic indium is reversibly reoxidized. The XRD spectra after oxidation do not show any metallic phase lines.

An endothermic peak around 157 °C is observed for the three samples, corresponding to the melting point of metallic indium. The peak is not well developed, because the oxidation occurs before it is finished. This can explain the two peaks observed in the oxidation process. The oxidation peak at low temperature is due to the oxidation of the melted indium. The newly generated indium oxide at this temperature is a solid that creates a layer over the rest of the metallic indium and prevents it from being oxidized. This metallic indium requires a higher temperature for oxidation.

3.2. De-NO_x catalytic activity

The In-based catalysts prepared on amorphous alumina were evaluated in the reduction of NO_x by C_2H_4 in oxygen-rich atmosphere at fixed contact time and variable temperature in the 250–550 °C interval. The catalyst activity was measured in terms of NO_x ($NO + NO_2$) conversion and selectivity. Selectivity was expressed in terms of the competitiveness factor, taking into account the catalyst's ability to selectively use the hydrocarbon to reduce the NO_x species rather than to be oxidized by O_2. The experimental results, in terms of reaction profiles of the main species involved in the de-NO_x reaction, are shown in Figs. 12a–12f for all of the catalysts as a function of reaction temperature. The addition of a very low amount of In is sufficient to impart new catalytic activity to the alumina support. Indeed, alumina is completely unable to reduce any NO_x under the same conditions used for studying the catalysts in the present work, and yields only a small amount of CO (about 10%) from ethene

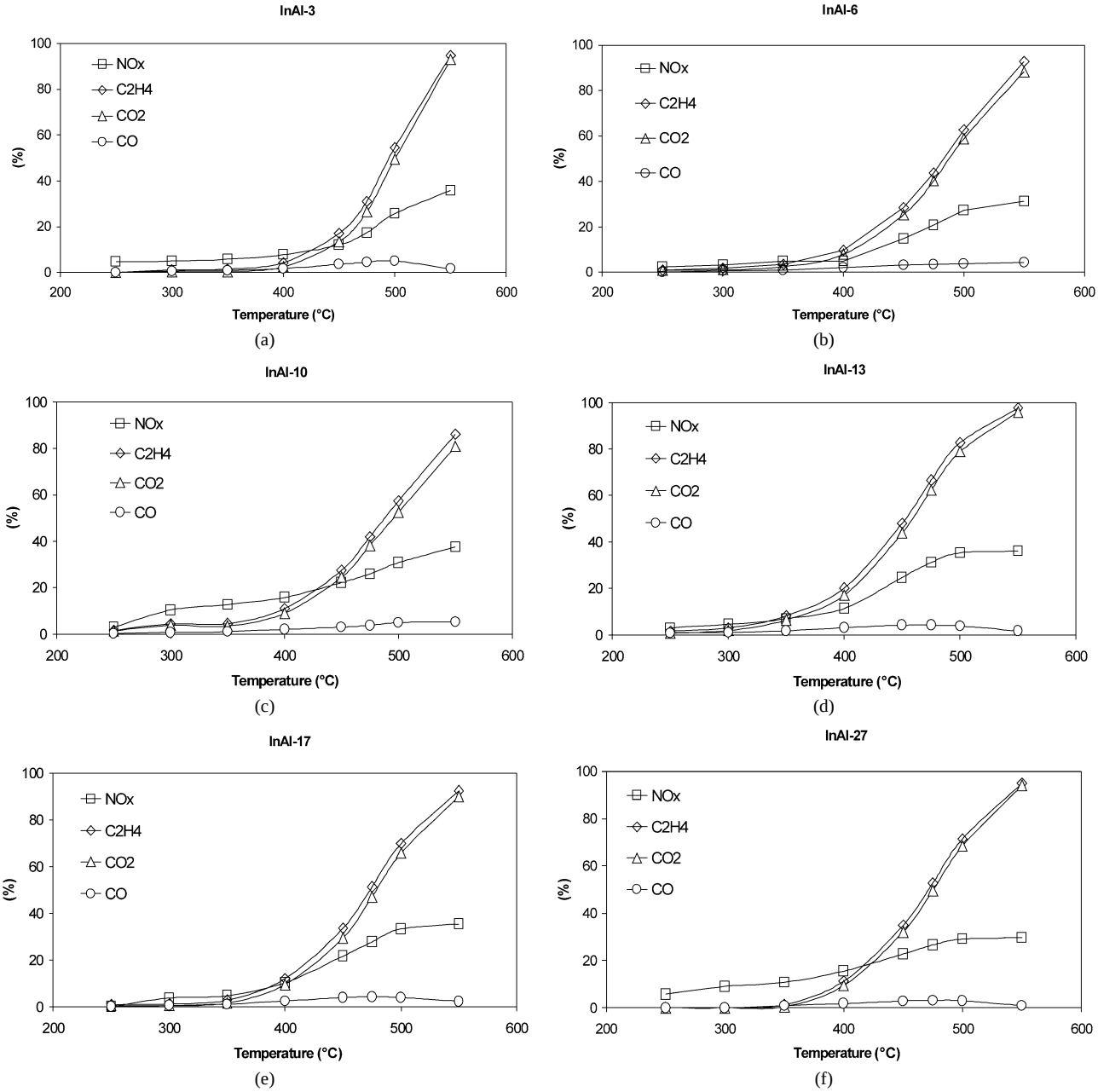

Fig. 12. Percentages of conversion of NO_x ($NO + NO_2$) and of C_2H_4, and percentages of formation of CO, and CO_2 as a function of reaction temperature in the NO_x reduction by C_2H_4 in O_2 at 1.6 g s mmol^{-1} of contact time: (a) InAl-3; (b) InAl-6; (c) InAl-10; (d) InAl-13; (e) InAl-17; and (f) InAl-27.

oxidation at higher temperatures. N_2O was not detected among the reaction products. This finding was expected, because it is known that the production of large amounts of N_2O in addition to N_2 is a specific distinctive feature of the reduction of NO_x on noble metal phases [50]. As a general trend, the onset temperature for the selective reduction of NO_x was around 400 °C. With the ability to detect the NO_2 species separately from NO, it was possible to observe in every case a significant NO_2 conversion at low temperatures that could be due to nitrite/nitrate accumulation over the surfaces. The subsequent decomposition of these primary formed species at higher temperatures could give rise to N_2 formation in some amount. The plots of the NO_x conversion versus temperature did not lead to volcano-shaped curves, as are usually observed for most de-NO_x catalysts. This behavior is due to the presence of ethene even at the highest reaction temperature tested. The incomplete ethene conversion at 500 °C and above can be associated with the weak oxidation properties of the In_2O_3 phase. This behavior can be quantified by computing the competitiveness factor, which represents the SCR selectivity (S_{SCR}, %). During the SCR reaction, the two oxidizing species, O_2 and NO_x, compete for the small amount of ethene present; at the highest reaction temperatures, O_2 prevails over NO_x, and S_{SCR} decreases abruptly. The good selectivity of the In_2O_3 phases is revealed by the S_{SCR} values, which attained 8–10% at the

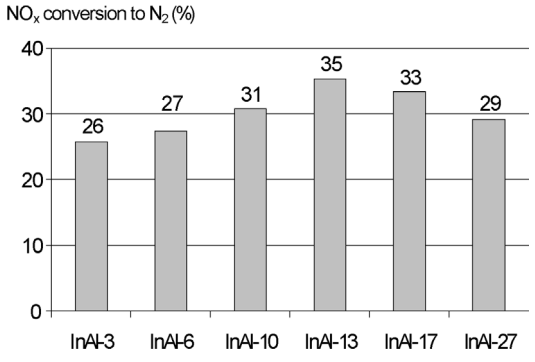

Fig. 13. Conversions of NO_x to N_2 compared over the different In-loaded samples at a reaction temperature of 500 °C.

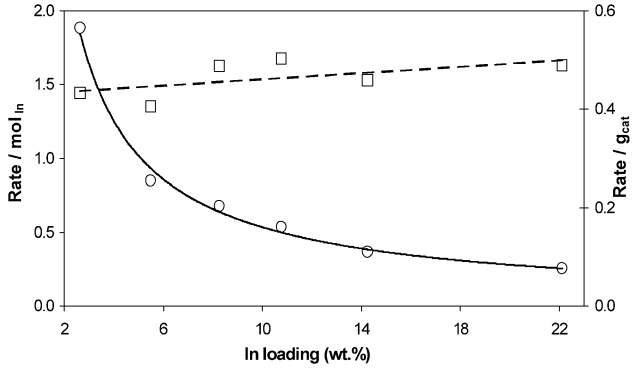

Fig. 14. Reaction rates in the C_2H_4-SCR of NO_x as a function of the In-loading expressed as $mmol_{N_2}\ mol_{In}^{-1}\ s^{-1}$ (rate/mol_{In}), circle markers, and in $\mu mol_{N_2}\ g_{cat}^{-1}\ s^{-1}$ (rate/g_{cat}), square markers, calculated at 500 °C.

highest reaction temperatures. In terms of carbon selectivity, ethene was converted to CO_2 for the most part, whereas only a very limited amount of CO was detected for temperatures around 450–500 °C (maximum yield, 3–4%). The carbon balance was very satisfactory in any case.

It is possible to compare the NO_x conversions over the various In_2O_3-based catalysts by considering their activities at a same reaction temperature. Fig. 13 shows the percentage of NO_x to N_2 conversion obtained from each catalyst evaluated at 500 °C; the same trend was observed if different temperatures were taken into account. The NO_x conversion increased with In_2O_3 loading up to 13%; from this point on, further In addition caused a decrease in conversion. The conversion of the InAl-27 sample was lower than that of the InAl-17 and InAl-13 samples.

The observed behavior suggests a key influence of the In surface aggregation on activity. Indeed, the sample with the lowest In concentration (InAl-3) is very active, and further addition of In resulted in a limited increase of the number of active In sites on the alumina support, thus generating no important variation in the de-NO_x activity.

On the basis of the experimental data obtained, specific integral reaction rates ($\mu mol_{N_2}\ g_{cat}^{-1}\ s^{-1}$) were calculated at each temperature. Moreover, from these values it is possible to express the rates in $mmol_{N_2}\ mol_{In}^{-1}\ s^{-1}$, once the amount of In per unit mass of catalyst is known. Fig. 14 shows the trend followed by these calculated rates as a function of In loading. It is more interesting to observe the values of the rates expressed per mol of In, which show a regularly decreasing exponential trend. This corroborates our suggestion concerning the role of In surface aggregation in de-NO_x activity. The addition of a very small amount of In_2O_3 to alumina is sufficient to impart good activity to the sample, whereas further In_2O_3 addition leads to samples with lower activity. This means that only a limited amount of the indium loaded over the alumina support can play the role of active site in NO_x reduction. This smaller amount could be associated with the fraction present at the surface of the In_2O_3 aggregates, which became larger as the In loading increased (see the XRD diffraction measurement results).

4. Conclusions

The deposition of indium oxide slightly decreases the acidic properties of alumina, but the amounts of ammonia adsorbed per m^2 of catalyst surface area do not vary significantly. Indium oxide deposition has a greater influence on the adsorption of acidic molecules; the adsorbed amount of SO_2 is related to the indium oxide surface content, not to the total deposited amount. The irreversible amount of SO_2 adsorbed is superior to the irreversible amount of NH_3 adsorbed, suggesting the presence of stronger basic sites on the indium-loaded samples. These findings suggest that indium oxide can be considered more basic than acidic.

Indium oxide is easily reduced, at a reduction temperature related to particle size. For smaller particles, the reduction begins around 200 °C. The reoxidation process starts at lower temperatures than the reduction process.

Balanced acidic and redox properties are indispensable for an efficient conversion of NO_x, that is, high activity and selectivity (over a broad temperature window). This evidence is in agreement with the conclusions drawn by Park et al. [37] claiming a bifunctional mechanism of the In_2O_3/Al_2O_3 systems to explain their high activity for NO_x reduction by propene. In this mechanism, the well-dispersed In sites activate the hydrocarbons into partially oxygenated compounds, and the acidic alumina sites readily use the oxygenated hydrocarbons to reduce NO_x.

In_2O_3 catalysts demonstrate good NO_x reduction performance at high temperatures compared with other active phases, such as CuO or SnO_2 [44,51–53], and in this sense they resemble Ga_2O_3-based catalysts [9,54]. With respect to alumina-based catalysts, the hydrocarbon oxidation and NO reduction activity have a strong mutual correlation, and, moreover, the interaction between In_2O_3 and alumina is necessary. The crystalline structure of the In_2O_3 phase observed on the high-In-loading catalysts is not associated with high de-NO_x activity, whereas small In_2O_3 aggregates well dispersed over the alumina support are active and selective in NO_x reduction. A balanced presence of indium and alumina sites indeed seems to be very important for achieving opti-

mal catalytic performance over this type of catalyst, confirming the first results published in the literature concerning the characterization and catalytic performance of In_2O_3/Al_2O_3 systems in NO_x reduction [37].

Acknowledgments

The authors thank Dr. Claude Guimon (Université de Pau et des Pays de l'Adour) for the XPS experiments, and the technical services of IRC for the XRD and chemical analyses.

References

[1] J. Ramirez, P. Castillo, L. Cedeno, R. Cuevas, M. Castillo, J.M. Palacios, A. Lopez-Agudo, Appl. Catal. A 132 (1995) 317.
[2] S.A. El-Hakam, A.A. El-Sharkaury, Mater. Lett. 36 (1998) 167.
[3] G. Colorio, J.C. Vedrine, A. Auroux, B. Bonnetot, Appl. Catal. A 137 (1996) 55.
[4] P.T. Wierzchowski, L. Zatorski, Appl. Catal. B 44 (2003) 53.
[5] B. Sulikowski, A. Kubacka, E. Wloch, Z. Schay, V. Cortés Corberán, R.X. Valenzuela, Stud. Surf. Sci. Catal. 130 (2000) 1889.
[6] M. Haneda, E. Joubert, J.C. Menezo, D. Duprez, J. Barbier, N. Bion, M. Daturi, J. Saussey, J.L. Lavalley, H. Hamada, Phys. Chem. Chem. Phys. 3 (2001) 1366.
[7] A.L. Petre, A. Auroux, A. Gervasini, M. Caldararu, N.I. Ionescu, J. Therm. Anal. Calorim. 64 (2001) 253.
[8] A.L. Petre, J.A. Perdigón-Melón, A. Gervasini, A. Auroux, Top. Catal. 19 (2002) 271.
[9] A.L. Petre, B. Bonnetot, A. Gervasini, A. Auroux, Stud. Surf. Sci. Catal. 143 (2002) 747.
[10] B. Gergely, A. Auroux, Res. Chem. Intermed. 25 (1999) 13.
[11] B. Gergely, A. Redey, C. Guimon, A. Gervasini, A. Auroux, J. Therm. Anal. Calorim. 56 (1999) 1233.
[12] T. Miyadera, K. Yoshida, Chem. Lett. (1993) 1483.
[13] T. Maunula, Y. Kintaichi, M. Inaba, M. Haneda, K. Sato, H. Hamada, Appl. Catal. B 15 (1998) 291.
[14] Y. Li, J.N. Armor, J. Catal. 145 (1994) 1.
[15] K. Shimizu, A. Satsuma, T. Hattori, Appl. Catal. B 16 (1998) 319.
[16] F.B. Passos, M. Schmal, M.A. Vannice, J. Catal. 160 (1996) 118.
[17] F.B. Passos, D.A.G. Aranda, M. Schmal, J. Catal. 178 (1998) 478.
[18] J. Li, J. Hao, L. Fu, T. Zhu, Z. Liu, X. Cui, React. Kinet. Catal. Lett. 80 (2003) 75.
[19] C. Schmidt, T. Sowade, F.-W. Schuetze, M. Richter, H. Berndt, W. Gruenert, Stud. Surf. Sci. Catal. 135 (2001) 4973.
[20] F.-W. Schütze, H. Berndt, M. Richter, B. Lucke, C. Schmidt, T. Sowade, W. Grünert, Stud. Surf. Sci. Catal. 135 (2001) 1517.
[21] E.E. Miró, L. Gutiérrez, J.M. Ramallo-López, F.G. Requejo, J. Catal. 188 (1999) 375.
[22] X. Wang, T. Zhang, X. Sun, W. Guan, D. Liang, L. Lin, Appl. Catal. B 24 (2000) 169.
[23] F.G. Requejo, J.M. Ramallo-López, E.J. Lede, E.E. Miró, L.B. Pierella, O.A. Annunziata, Catal. Today 54 (1999) 553.
[24] H. Berndt, F.-W. Schütze, M. Richter, T. Sowade, W. Grünert, Appl. Catal. B 40 (2003) 51.
[25] M. Iwamoto, H. Hamada, Catal. Today 10 (1991) 57.
[26] M. Iwamoto, H. Yahiro, N. Mizuno, S. Kagawa, Chem. Lett. (1989) 213.
[27] E. Kikuchi, K. Yogo, Catal. Today 22 (1994) 73.
[28] H.Y. Chen, W.M.H. Sachtler, Catal. Lett. 50 (1998) 125.
[29] E. Kikuchi, M. Ogura, I. Terasaki, Y. Goto, J. Catal. 161 (1996) 465.
[30] K. Yogo, M. Ihara, I. Terasaki, E. Kikuchi, Appl. Catal. B 2 (1993) L1.
[31] X. Zhou, T. Zhang, Z. Xu, L. Lin, Catal. Lett. 40 (1996) 35.
[32] M. Serban, I. Halasz, R. Datta, Catal. Lett. 63 (1999) 217.
[33] H. Hamada, Y. Kintaichi, M. Sasaki, T. Ito, M. Tabata, Appl. Catal. 75 (1991) L1.
[34] T. Tabata, H. Hamada, F. Suganuma, T. Yoshinari, H. Tsuchida, Y. Kintaichi, M. Sasaki, T. Ito, Catal. Lett. 25 (1994) 55.
[35] H. Hamada, Y. Kintaichi, T. Yoshinari, M. Tabata, M. Sasaki, T. Ito, Catal. Today 17 (1993) 112.
[36] S. Subramanian, R.J. Kudla, W. Chun, M.S. Chattha, Ind. Eng. Chem. Res. 32 (1993) 1805.
[37] P.W. Park, C.S. Ragle, C.L. Boyer, M.L. Balmer, M. Engelhard, D. McCready, J. Catal. 210 (2002) 97.
[38] M. Haneda, E. Joubert, J.C. Ménézo, D. Duprez, J. Barbier, N. Bion, M. Daturi, J. Saussey, J.C. Lavalley, H. Hamada, J. Mol. Catal. A 175 (2001) 179.
[39] N. Cardona-Martinez, J.A. Dumesic, Adv. Catal. 38 (1992) 149.
[40] E. Farneth, R.J. Gorte, Chem. Rev. 95 (1995) 615.
[41] A. Auroux, Top. Catal. 4 (1997) 71.
[42] A. Auroux, Top. Catal. 19 (2002) 205.
[43] R.C. Weast, D.R. Lide, M.J. Astle, W.H. Beyer (Eds.), Handbook of Chemistry and Physics, seventieth ed., CRC Press, Boca Raton, FL, 1989–1990.
[44] A. Auroux, D. Sprinceana, A. Gervasini, J. Catal. 195 (2000) 140.
[45] K.A. Bethke, M.C. Kung, B. Yang, M. Shah, D. Alt, C. Li, H.H. Kung, Catal. Today 26 (1995) 169.
[46] S.K. Poznyak, A.N. Golubev, A.I. Kulak, Surf. Sci. 454–456 (2000) 396.
[47] M.I. Zaki, M.A. Hasan, F.A. Al-Sagheer, L. Pasupulety, Colloids Surf. A 190 (2001) 261.
[48] S.M. Maurer, D. Ng, E.I. Ko, Catal. Today 16 (1993) 319.
[49] R.M. Mihályi, H.K. Beyer, V. Mavrodinova, Ch. Minchev, Y. Neinska, Micropor. Mesopor. Mater. 24 (1998) 143.
[50] R. Burch, P.J. Millington, Catal. Today 26 (1995) 185.
[51] C. Guimon, A. Gervasini, A. Auroux, J. Phys. Chem. 105 (2001) 10316.
[52] P. Carniti, A. Gervasini, V.H. Modica, N. Ravasio, Appl. Catal. B 28 (2000) 175.
[53] S. Bennici, A. Gervasini, N. Ravasio, F. Zaccheria, J. Phys. Chem. B 107 (2003) 5168.
[54] M. Haneda, Y. Kintaichi, T. Mizushima, N. Kakuta, H. Hamada, Appl. Catal. B 31 (2001) 81.